Article

Cell Reports

Defining Midbrain Dopaminergic Neuron Diversity by Single-Cell Gene Expression Profiling

Graphical Abstract

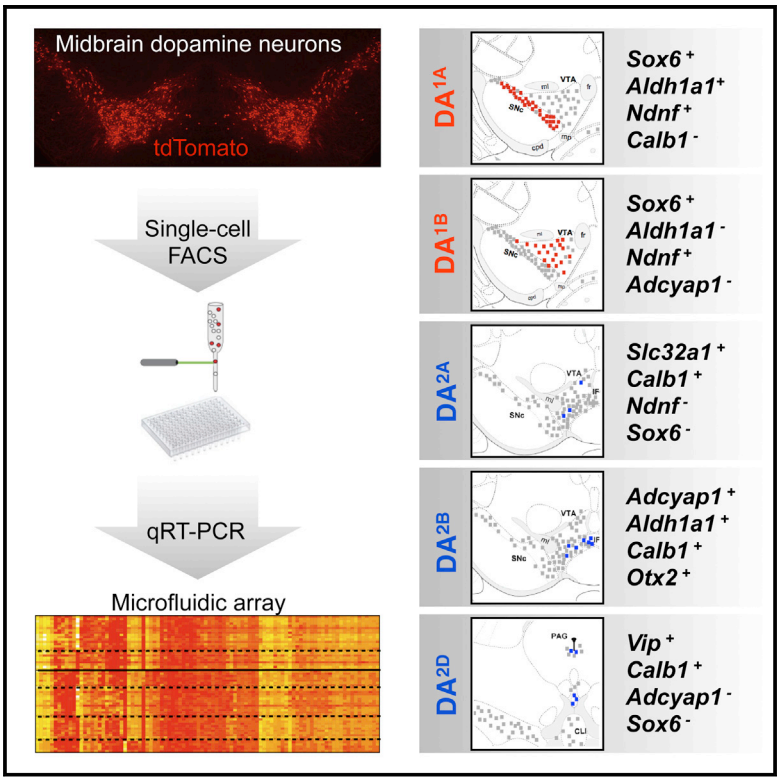

Authors

Jean-Francois Poulin, Jian Zou, ..., Francesca Cicchetti, Rajeshwar B. Awatramani

Correspondence

r-awatramani@northwestern.edu

In Brief

Poulin et al. used a single-cell gene-profiling approach to identify multiple molecularly distinct midbrain dopamine neuron subtypes. The findings have implications for targeted therapeutics of dopamine-related diseases understanding the differential vulnerability of dopamine neurons, generating stem-cell-derived dopamine neurons, and understanding the dopaminergic system by providing points of genetic access.

Highlights

Single-cell gene profiling identified multiple midbrain dopamine neuron subtypes

A *Vip*-expressing subtype projects to specific nuclei within the extended amygdala

A subtype expressing *Aldh1a1* is more vulnerable in a model of Parkinson's disease

Poulin et al., 2014, Cell Reports 9, 930–943
November 6, 2014 ©2014 The Authors
http://dx.doi.org/10.1016/j.celrep.2014.10.008

OPEN ACCESS
CellPress

Cell Reports
Article

Defining Midbrain Dopaminergic Neuron Diversity by Single-Cell Gene Expression Profiling

Jean-Francois Poulin,[1] Jian Zou,[1] Janelle Drouin-Ouellet,[2] Kwang-Youn A. Kim,[3] Francesca Cicchetti,[4] and Rajeshwar B. Awatramani[1,*]

[1]Department of Neurology and the Center for Genetic Medicine, Northwestern University, Chicago, IL 60611, USA
[2]John van Geest Centre for Brain Repair, University of Cambridge, Cambridge CB2 0PY, UK
[3]Department of Preventive Medicine, Feinberg School of Medicine, Northwestern University, Chicago, IL 60611, USA
[4]Centre de Recherche du CHU de Québec, Axe Neurosciences and Université Laval, Québec, QC G1V 4G2, Canada
*Correspondence: r-awatramani@northwestern.edu
http://dx.doi.org/10.1016/j.celrep.2014.10.008

SUMMARY

Effective approaches to neuropsychiatric disorders require detailed understanding of the cellular composition and circuitry of the complex mammalian brain. Here, we present a paradigm for deconstructing the diversity of neurons defined by a specific neurotransmitter using a microfluidic dynamic array to simultaneously evaluate the expression of 96 genes in single neurons. With this approach, we successfully identified multiple molecularly distinct dopamine neuron subtypes and localized them in the adult mouse brain. To validate the anatomical and functional correlates of molecular diversity, we provide evidence that one Vip+ subtype, located in the periaqueductal region, has a discrete projection field within the extended amygdala. Another Aldh1a1+ subtype, located in the substantia nigra, is especially vulnerable in the 1-methyl-4-phenyl-1,2,3,6-tetrahydropyridine (MPTP) model of Parkinson's disease. Overall, this rapid, cost-effective approach enables the identification and classification of multiple dopamine neuron subtypes, with distinct molecular, anatomical, and functional properties.

INTRODUCTION

The mammalian CNS is an extremely heterogeneous organ composed of hundreds of neuronal and nonneuronal cell types (Ng et al., 2009). There is an urgent need to transition from cell groups, traditionally defined by cytology and anatomy, to molecularly defined cell types in order to generate a comprehensive catalog of the mammalian CNS (Bota and Swanson, 2007; Fishell and Heintz, 2013). In this regard, several in situ hybridization and transgene-profiling studies have served as an important step in classification of neurons in given brain regions (Shimogori et al., 2010; Siegert et al., 2009).

The next important step toward classifying cellular diversity requires the analysis of a multitude of markers with single-cell resolution. Molecular definition of neurons should rely on a polythetic approach, rather than stochastically expressed markers (Bota and Swanson, 2007). This transition is mandatory for accurately defining neuronal circuitry and its relation to complex neural functions and behaviors. An ideal approach to investigate neuronal diversity would allow a quick, reliable, and quantitative assessment of the gene-expression profile of single neurons obtained from the mammalian brain. Although recent reports of single-cell transcriptomics have been published, this approach is cost prohibitive and has yet to reach its maturity before being broadly applicable to the mammalian CNS (Macaulay and Voet, 2014; Tang et al., 2010; Xue et al., 2013). As an alternative technology to simultaneously profile multiple genes from a single cell, we used a microfluidic chip array to investigate neuronal diversity from mouse brain.

We focused on the investigation of the clinically important midbrain dopaminergic (DA) system. Midbrain DA neurons influence a large spectrum of behaviors, and DA dysfunction is prominently implicated in a wide variety of disorders including Parkinson's disease (PD), schizophrenia, attention deficit hyperactivity disorder (ADHD), obsessive-compulsive disorder, addiction, and depression, together affecting tens of millions of people. How a small group of neurons, constituting less than 1% of brain neuronal populations, can account for such diverse physiological functions has been a subject of interest since their discovery. We hypothesized that multiple molecularly distinct DA subtypes could be partly responsible for the functional diversity of the DA system.

During embryonic development, midbrain DA neurons are derived from the Shh+ floor plate (FP) (Blaess et al., 2011; Hayes et al., 2011; Joksimovic et al., 2009; Kittappa et al., 2007). FP progenitors already display some heterogeneity, in terms of gene expression and proclivity to contribute to distinct nuclei (Blaess et al., 2011; Hayes et al., 2011; Joksimovic et al., 2009; Wallén et al., 1999). Immature DA neurons migrate from the ventricular zone into the mantle and express a series of transcription factors and other genes, some of which are heterogeneously expressed in the nascent DA cohort (Ang, 2006; Chung et al., 2010; Di Salvio et al., 2010a; Smidt and Burbach, 2007; Smits et al., 2013). Thus, the earliest aspects of DA neuron heterogeneity appear to be established in the early embryo, although it is likely that subsequent maturation events build on, or refine, DA heterogeneity. This model is akin to that proposed for the generation of

cortical interneuron lineages, wherein embryonic cardinal classes are established, and sequentially refined, to generate the full repertoire of interneurons (Kepecs and Fishell, 2014).

When considering the possibility of distinct postnatal DA neuron populations, the overwhelming literature is based on anatomical classification of midbrain DA neurons to three clusters: the substantia nigra pars compacta (SNc) (A9), the ventral tegmental area (VTA) (A10), and a third smaller cluster, found in the retrorubral area (RR) (A8). Accordingly, several studies have addressed the molecular heterogeneity of DA neurons in anatomically defined SNc versus VTA populations with microarray analysis (Chung et al., 2005; Greene et al., 2005; Grimm et al., 2004). Although informative, these studies rely on the premise that the SNc and VTA are composed of molecularly homogeneous populations. Considering the diverse functions of this neurotransmitter system and recent reports of physiological and functional heterogeneity (Darvas and Palmiter, 2009; Di Salvio et al., 2010b; Ekstrand et al., 2014; Guzman et al., 2010; Lammel et al., 2008, 2012; Margolis et al., 2006a, 2006b; Stamatakis et al., 2013; Tye et al., 2011), we postulated the existence of several molecularly distinct DA neuron subtypes, which may not necessarily be segregated anatomically but rather may be intermingled with one another. Providing the molecular identity of DA neuron subtypes would have meaningful implications for (1) targeted therapeutics of the DA system, (2) understanding the differential vulnerability of DA neurons, (3) developing more-accurate stem-cell- and induced-pluripotent-stem-cell-derived DA neurons, and (4) a deeper understanding of the DAergic system by providing points of genetic access, thus allowing genetic dissection of this neurotransmitter system.

RESULTS

Comprehensive Single-Cell Gene-Expression Profile of Midbrain Dopamine Neurons

To redefine the DA system on a molecular basis, we devised a neuroanatomically unbiased systematic approach to profile single midbrain DA neurons. We opted for a 96.96 dynamic array to evaluate 96 cells, each for the expression of 96 key genes, an approach used previously to discriminate stem cell identities (Buganim et al., 2012; Guo et al., 2010). We selected 96 gene candidates based on reported differential expression between SNc and VTA (Chung et al., 2005; Greene et al., 2005; Grimm et al., 2004), with a positive bias toward genes with validated midbrain mRNA expression as shown by in situ hybridization in public databases (Table S1). In addition, we evaluated the expression of housekeeping genes (*Actb*, *Gapdh*, and *Hprt*), genes linked to PD (*Atp13a2*, *Lrrk2*, *Park2*, *Park7*, *Pink1*, and *Snca*), as well as validated DA neuronal markers (*Ddc*, *Th*, *Slc6a3*, and *Slc18a2*). All primers used were prevalidated using serial dilution of commercial reference samples. To isolate single DA neurons, we grossly dissected and dissociated the midbrain of postnatal day 4 (P4) *Slc6a3*::*Cre*, Ai9 mice. These mice have been described previously (Bäckman et al., 2006; Madisen et al., 2010) and, in our hands, resulted in more than 95% of Th+ midbrain DA neurons expressing tdTomato following Cre-dependent recombination. Fluorescently labeled single cell expressing tdTomato were sorted into 96-well plates with fluorescence-activated cell sorting (FACS; Figure 1A). P4 was selected as a specific time point, in part because of the technical ease of FACS at this stage (Arlotta et al., 2005). Supporting this choice, it has been argued that neuronal molecular identity is established shortly after cells exit their last mitotic cycle (Fishell and Heintz, 2013). Indeed, the vast majority of markers that we selected are expressed in the developing embryo or in the neonate, supporting P4 as a meaningful time point (Hoekstra et al., 2013; Veenvliet et al., 2013).

In the initial experiment, 87 single cells were sorted in a 96-well plate for gene-expression analysis (Figure 1B). The remaining nine wells included a brain cDNA dilution series to generate a standard curve. The Biomark microfluidics chip allows the combination of samples and primer probe sets for 9,216 quantitative RT-PCR reactions with cycle threshold (Ct) values as output (Figure S1). For quality control purposes, the melting curve of every reaction was determined, and every reaction with a peak falling outside the expected value was removed from the analysis (examples of standard curve and melting curve are provided in Figure S2). This experiment was replicated by two other arrays filled with single cells sorted from two additional mice. Using a cutoff criterion of two SDs away from the median of the housekeeping gene *Gapdh* and key DA neurons defining genes *Th*, *Slc6a3* (Dat), *Slc18a2* (Vmat2), and *Ddc* (Aaad), we removed all cells exhibiting a weak and unreliable expression. Altogether, we were left with 159 DA neurons for further analysis, and the complete expression profile of these cells is provided in Figure S3. All these neurons had expression of key transcription factors such as *Foxa1*, *En1/2*, *Lmx1b*, *Pitx3*, and *Nr4a2*; because the combinatorial expression of these transcription factors is unique to midbrain DA neurons, their expression confirms the absence of hypothalamic DA neurons in the FACS-sorted cells. Additionally, all samples had virtually undetectable levels of *Gad1*, confirming the absence of GABAergic neurons.

From gene-expression data (Figures 1B and S3), it is apparent that a large number of genes are expressed in all DA neurons. The genes expressed in most DA neurons include PD-linked genes *Atp13a2*, *Lrrk2*, *Park2*, *Park7*, and *Pink1*, as well as the transcription factors *Foxa1*, *En1/2*, *Lmx1b*, *Pitx3*, and *Nr4a2*. In contrast to these uniformly expressed genes, several genes are differentially expressed between individual DA neurons. As an approach for investigating molecular heterogeneity of DA populations, we used an unbiased coefficient similarity hierarchical clustering analysis to parcel these cells according to their gene-expression profile (Figures 1B and S4). This analysis revealed the presence of two main clusters that could be further divided into a total of six molecularly distinct DA subtypes (Figure 2A). Out of 159 cells, 55 cells (35%) belong to the first cluster, 98 cells (61%) were assigned to the second cluster, whereas six cells (4%) could not be assigned. The first cluster can be subdivided into two subtypes, here referred to as DA^{1A} and DA^{1B}, which are composed of 33 cells (21%) and 22 cells (14%), respectively. The second cluster can be subdivided into four molecularly distinct subtypes labeled DA^{2A} (18%), DA^{2B} (23%), DA^{2C} (12%), and DA^{2D} (9%). Interestingly, these six molecular subtypes were represented in a roughly similar proportion in all three microfluidic arrays (Figure 2A).

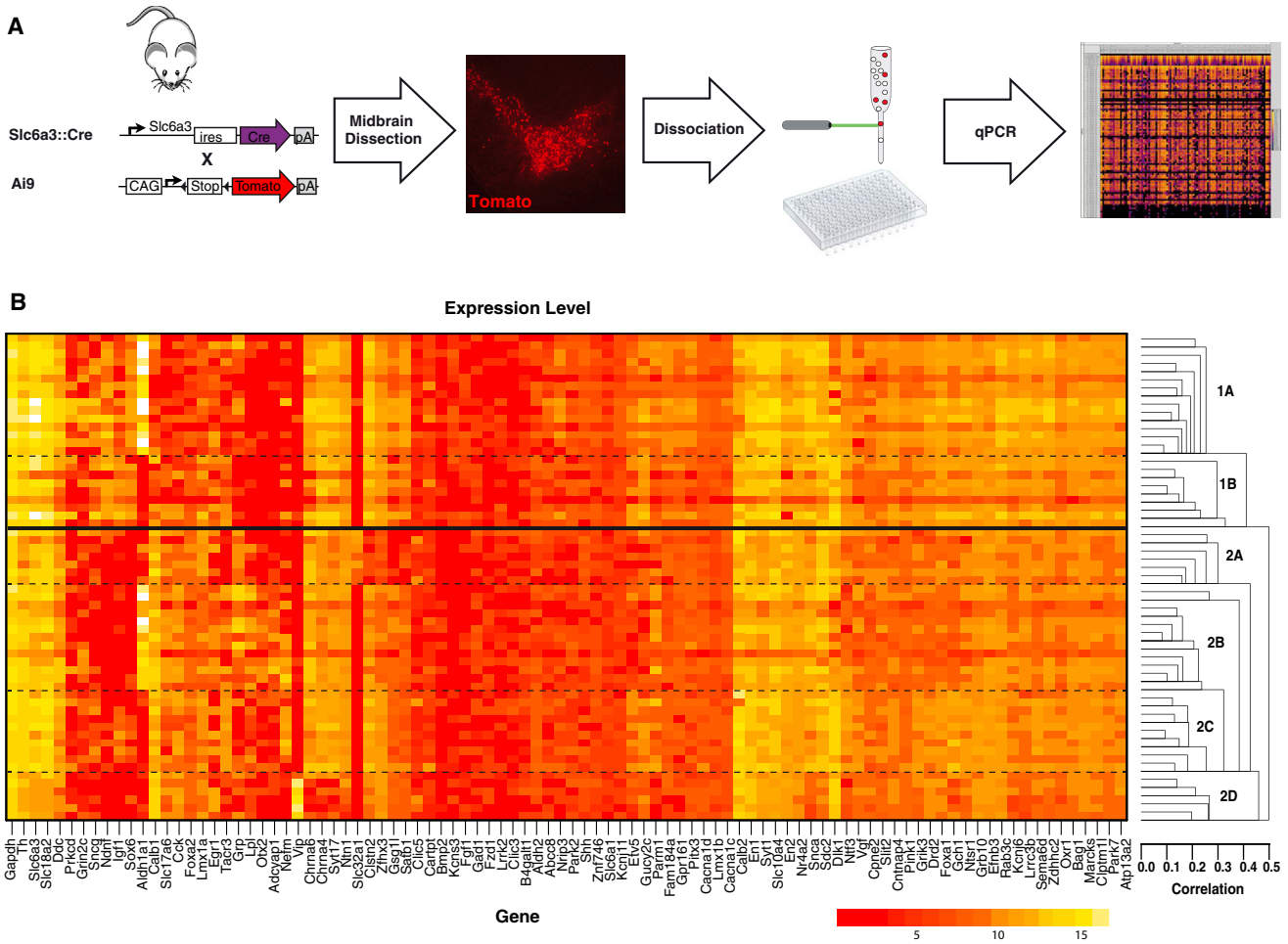

Figure 1. High-Throughput Single-Cell Gene-Expression Analysis of Midbrain Dopamine Neurons

(A) The midbrain of postnatal day 4 *Slc6a3*::*Cre*; Ai9 was dissected and dissociated. Fluorescent (tdTomato+) single cells were FACS sorted into 96-well plates and analyzed for the expression of 96 genes using Fluidigm Biomark system.

(B) A sample array in which the expression level of each gene is depicted on a logarithmic scale with red indicating low expression and yellow representing a high expression. Unbiased clustering analysis revealed the presence of two main clusters that could be further divided into a total of six molecularly distinct dopamine (DA) neuron subtypes.

We compared the relative gene-expression level, normalized to *Gapdh*, of the two identified main clusters by subtracting the average value of cells assigned to the second cluster to the average value of cells assigned to the first cluster (Figure 2B). *Gapdh* proved to be a reliable housekeeping gene because there were significant correlations between this gene and other known housekeeping genes, *Actb* ($r = 0.939$; $n = 105$; $p < 0.0001$) and *Hprt* ($r = 0.922$; $n = 105$; $p < 0.0001$). This analysis revealed significant differences between these clusters in the expression of some key genes. For instance, *Sox6*, *Slc6a3*, *Zdhhc2*, and *Nrip3* have a higher expression in the first compared to the second cluster. Interestingly, those four genes were previously reported to have a higher expression in pooled cells of the SNc compared to the VTA (illustrated in red in Figure 2B; see Table S1 for references). In comparison, we found that *Calb1*, *Slc17a6*, *Cck*, *Calb2*, and *Efnb3* are five genes found to have a higher expression in the second cluster. These five genes, like the majority of genes overexpressed in the second cluster, were previously associated with cells of the VTA (illustrated in blue in Figure 2B; see Table S1 for references). It is important to note that cells were not identified based on their neuroanatomical position, because the anatomical origin of each FACS-sorted cell is undetermined. However, we can conclude that the expression profile of cells from cluster 1 has more similarity with the molecular signature of cells of the SNc, whereas cells from cluster 2 have an expression profile related to the VTA. This prediction is indeed borne out in subsequent anatomical analysis, which shows that DA^{1A} and DA^{1B} (cluster 1) are more localized to the SNc, whereas DA^{2A}–DA^{2D} (cluster 2) are preferentially localized to the VTA.

Molecular Signature of Dopamine Neuron Subtypes

The DA neuron subtypes defined by clustering analysis harbor an organized gene-expression profile, which can be used to derive

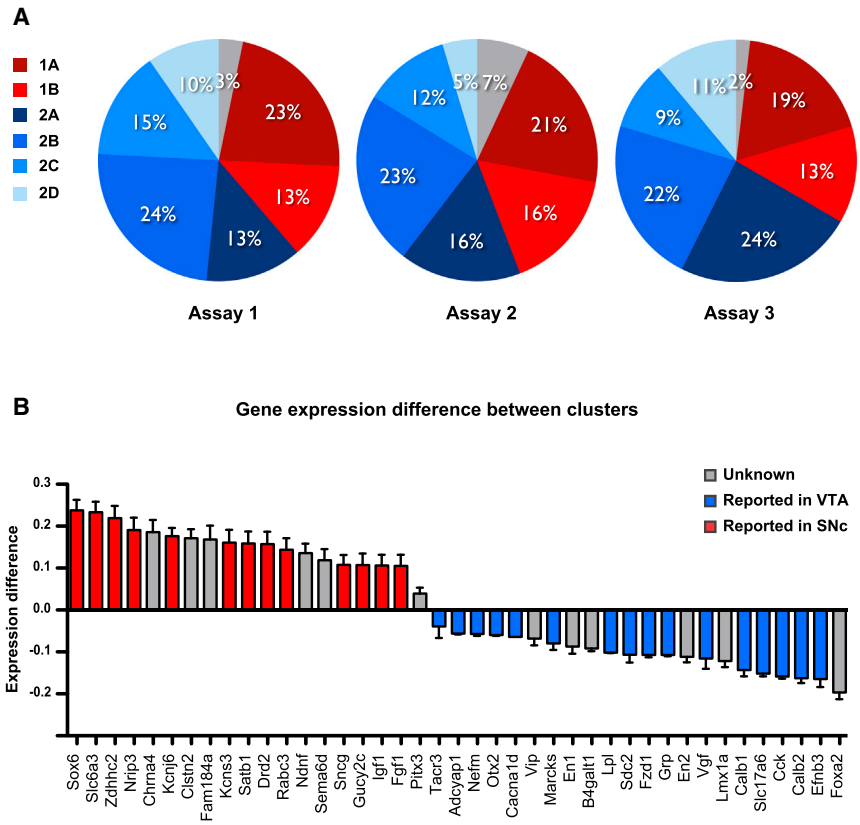

Figure 2. Dopamine Neurons Cluster into Distinct Subtypes

(A) Out of 159 cells, 55 cells (35%) belong to the first cluster, 98 cells (61%) were assigned to the second cluster, whereas six cells (4%) could not be assigned. Overall, clustering analysis identified six DA subtypes, represented in a roughly similar proportion in all three microfluidic arrays. The first cluster can be subdivided into two subtypes, referred to as DA^{1A} and DA^{1B}, which are composed of 33 cells (21%) and 22 cells (14%), respectively. The second cluster can be subdivided into four molecularly distinct subtypes, labeled DA^{2A} (18%), DA^{2B} (23%), DA^{2C} (12%), and DA^{2D} (9%).

(B) We compared the gene-expression level normalized to *Gapdh* between the two identified clusters. Genes previously reported to be overexpressed in the VTA are illustrated in blue and genes overexpressed in the SNc illustrated in red (see Table S1 for references). This quantitative analysis demonstrates the similarity between the gene-expression profile of cluster 1 and previously reported profile of SNc, as well as the similarity between cluster 2 and previously reported profile of the VTA.

All error bars are SEM.

a molecular bar code unique to each subtype (Figure 3). To gain further insight into the data, we used principal-component analysis (PCA) to identify components responsible for the variance observed. Applied to the expression data of the 159 cells, we extracted four principal components (PCs) and found that the first principal component (PC1) underlies 22.1% of the observed variance, PC2 contributes 13.8% to the variance, whereas PC3 and PC4 contribute to 8.7% and 6.7% of the variance, respectively. Together, these four PCs account for more than 50% of the variation of the data set. The first cluster is divided into DA^{1A} and DA^{1B} and both express high levels of *Ndnf*, *Sox6*, and *Sncg* mRNA, and the loading of these genes' contribution to PC1 are 0.237 (*Ndnf*), 0.232 (*Sox6*), and 0.145 (*Sncg*; Figures 3A, 3B, and S5A). However, the high expression of *Aldh1a1* in DA^{1A}, a gene absent from DA^{1B}, as well as the higher expression of *Snca* gene, allowed us to differentiate these two populations (Figures 3A and 3B). In contrast, *Igf1* is more highly expressed in DA^{1B} compared to DA^{1A}. Interestingly, all these genes contribute significantly to PC3 and thus allowed us to segregate those two populations by PCA (Figure 3A).

In order to validate these results and anatomically localize these DA subtypes in the adult midbrain, we used a combination of immunofluorescence, fluorescent in situ hybridization, and transgenic mice. The majority of DA^{1A} neurons are located in the ventral tier of the SNc (Figure 4A), with a few cells observed in RR. In those two regions, Aldh1a1 labels 36.7% ± 1.8% and 12.1% ± 2.3% of DA neurons, respectively, overall accounting for approximately 15.4% ± 1.3% of all midbrain DA neurons. Within the DAergic field, Aldh1a1 antibody overwhelmingly labeled DA neurons (Figure S6), with occasionally one cell per section appearing negative for Th. Within the SNc, Aldh1a1+ neurons are located in the ventral tier and are also immunolabeled by Sncg and Sox6 but are not labeled with Calb1 and Otx2 antibodies (Figure 4A). These neurons also coexpressed *Aldh1a1* and *Sncg* mRNA, which is in complete agreement with our single-cell expression profile of DA^{1A} cells (Figure 3A). Indeed, according to the array, only the DA^{1A} subtype expresses a combination of *Aldh1a1*, *Sox6*, and *Sncg* but do not express *Otx2* and *Calb1*. In contrast to DA^{1A}, DA^{1B} neurons are located in the dorsal part of the SNc and intermingled with other DA subtypes in the rostro-dorsal VTA (Figure 4B). These neurons are Sox6+ and Sncg+ but negative for Aldh1a1. Moreover, Calb1 was variably expressed in Sox6-positive cells of DA^{1B}, which also appear to mirror the single-cell array data, whereby varying levels of *Calb1* mRNA were detected in this population.

The second cluster can be defined by a particularly high expression of *Calb1*, *Slc17a6*, and *Cck*, among others, and can be further divided into four DA subtypes (DA^{2A}–DA^{2D}), each defined by a unique molecular signature (Figures 3C–3F). Subtype DA^{2A} is specifically defined by the expression of the GABA vesicular transporter *Slc32a1* (also known as *Vgat*), because this gene is not significantly expressed by any other subpopulation (Figures 3C and S5A). This opens the intriguing possibility that DA^{2A} may corelease GABA, and it is conceivable that this subtype matches a described DA population sending an inhibitory projection to the lateral habenula (Stamatakis et al., 2013). Notably, these cells did not reliably express *Gad1*, a key GABA synthesis gene, ruling out the possibility of GABAergic

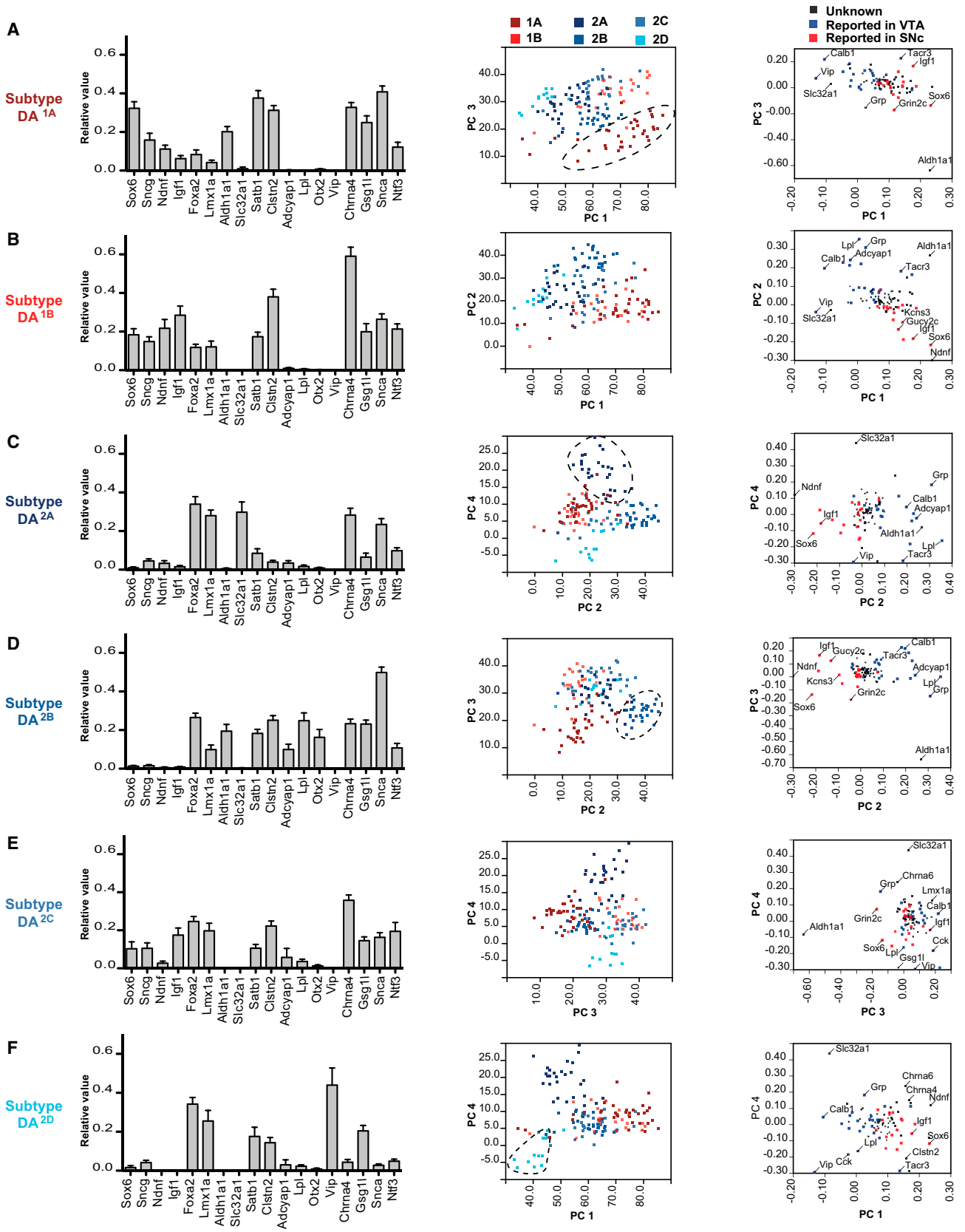

(legend on next page)

neuron contamination. This DA subtype is also uniquely defined by low expression of a list of genes, which includes *Th*, *Satb1*, *Clstn2*, *Gsg1l*, *Zfhx3*, and *Tacr3* (Figure S5). Interestingly, all these genes contribute significantly to PC4, which allowed us to segregate DA^{2A} from the other populations (Figure 3C). In order to validate the molecular bar code obtained from our single-cell approach, we aimed at localizing DA^{2A} neurons in the adult brain. Because Slc32a1 immunoreactivity is localized in dendrites and is also present in GABAergic neurons, coimmunolabeling analyses proved challenging. Therefore, we crossed *Slc32a1*::*Cre* knockin line to a nuclear LacZ (nLacZ) reporter (Figure 5A; see Experimental Procedures for details). Although nLacZ was present in a large number of neurons, presumably GABAergic, confocal analysis revealed in some cells the colocalization of nLacZ with several markers of midbrain DA neurons including *Th*, *Nr4a2*, and *FoxA2* as shown in Figure 5A. These neurons were found to be intermingled with other cell types within the VTA, interfascicular nucleus (IF), and caudal linear nucleus (CLI) regions. Quantification of nLacZ and Nr4a2 colabeled cells shows that subtype DA^{2A} might comprise approximately 14.4% ± 3.8% of DA neurons of the VTA but only about 10% of the IF/CLI. We also observed the colocalization of *Slc32a1* and *Th* mRNA, supporting our single-cell quantitative PCR (qPCR) and *Slc32a1*::*Cre* recombination data (Figure 5A).

Subpopulation DA^{2B} is uniquely defined by high/exclusive expression of *Lpl*, *Otx2*, and *Adcyap1* as well as *Grp* (Figures 3D and S5). These genes contribute strongly to PC2 to the order of 0.355 (*Lpl*), 0.221 (*Otx2*), 0.242 (*Adcyap1*), and 0.309 (*Grp*). This population displays also strong expression of *Aldh1a1* but, contrary to DA^{1A}, which also expresses *Aldh1a1*, DA^{2B} depicts high levels of *Calb1* and other molecular determinant of the second cluster. Subtype DA^{2B} can be isolated by plotting cells according to PC3 and PC2 (Figure 3D). We validated the localization of some of those markers in the adult mouse brain. We could locate subtype DA^{2B} neurons by colabeling of Aldh1a1 and Otx2 (Figure 5B), a combinatorial code unique to this DA subtype. Aldh1a1+ neurons composed approximately 18.7% ± 2.4% of the DA neurons of the VTA, 52.3% ± 5.1% of the IF, and 17.5% ± 2.3% of the CLI. Together, Aldh1a1+ neurons in these regions account for 11.3% ± 1.3% of all midbrain DA neurons. The marker Otx2 is less specific to DA neurons with numerous Th-negative cells observed within the VTA and neighboring regions (e.g., interpeduncular nucleus; Figure 5B). Within the VTA, IF, and CLI, more than 60% of Aldh1a1-labeled DA neurons were also positive for Otx2. These cells contain high levels of Calb1 but are negative for Sox6 and Sncg (not shown), which confirms the single-cell expression profile obtained with the array. This Grp+ DA^{2B} population matches a recently described DA population that projects to the nucleus accumbens (Ekstrand et al., 2014).

In comparison to other DA subtypes, DA^{2C} is harder to define molecularly because it is not uniquely distinguished by expression of a single gene like other subtypes of the second cluster. All genes characterizing the second cluster are strongly expressed in this population (e.g., *Calb1*, *Cck*, and *Slc17a6*), but none of the markers identifying other subpopulations are present: *Slc32a1* (DA^{2A}), *Adcyap1* (DA^{2B}), and *Vip* (DA^{2D}; Figure 3E). Interestingly, genes characterizing cluster 1 are also expressed in this subpopulation, albeit at lower levels (e.g., *Sox6* and *Igf1*, but not *Ndnf*). Not surprisingly, this subtype could not be isolated by PCA (Figure 3E). It is also possible that DA^{2C} could be comprised of multiple DA subtypes that are indistinguishable by our analyses.

The final DA subtype identified, DA^{2D}, depicts a unique and well-defined gene-expression profile with the exclusive expression of *Vip* (Figure 3F) combined to low/absent expression of *Snca*, *Chrna4*, and *Ntf3* (Figures 3F and S5A). Like most cells belonging to cluster 2, these cells express *Calb1*, *Cck*, and *Foxa2* but do not express *Sox6* and *Ndnf*. In the adult mouse brain, these neurons are located in the periaqueductal gray (PAG) and dorsal raphe nucleus (Figure 5C). Within the PAG, we observed that, in the *Slc6a3*::*Cre*/Ai9 mouse, about 48.7% ± 1.2% of tdTomato-positive cells expressed Vip. On the other hand, 50.0% ± 1.3% of Vip+ cells were labeled with tdTomato, suggesting that some cells of this population could have evaded recombination due to very low Slc6a3 expression level. Vip-labeled DA neurons coexpress most DAergic markers including Th and FoxA2, but little to no expression of Sox6, Sncg, Aldh1a1, and Otx2 (Figure 5C; data not shown) was detected by immunofluorescence in the adult brain. Interestingly, for subtype DA^{2D}, we were able to take advantage of strong Vip immunolabeling to visualize its projections in *Slc6a3*::*Cre*; Ai9 mice (Figure 5D). Vip immunoreactivity is found only in a subset of the DA projections. Whereas DA projections are extensive in the extended amygdala, Vip immunolabeling is only observed in the oval portion of the bed nucleus of the stria terminalis (BSTov) and the lateral portion of central nucleus of the amygdala (CEAl). High-magnification images of fibers depict the colocalization of Vip and tdTomato in axonal boutons of DA neurons terminating in the BSTov and CEAl (Figure 5D, inset). Vip labeling is excluded from other DA fields including the lateral septum (Figure 5D), striatum, accumbens, and cortex. This labeling is consistent with retrograde tracer analysis showing a dopaminergic projection from the PAG/dorsal raphe (DR) directed toward the

Figure 3. The Distinctive Molecular Signatures of the Six Dopamine Neuron Subtypes

The normalized expression profile of the six DA neuron subtypes is illustrated using 18 key genes. Plotting cells on the four extracted components of the principal-component analysis allows the differentiation of most DA subtypes.

(A) DA^{1A} is the only subtype with high expression of *Aldh1a1*, *Sox6*, and *Ndnf* and low expression of *Foxa2* and *Lmx1a*.

(B) DA^{1B} depicts an expression profile similar to DA^{1A} but lacks *Aldh1a1* expression.

(C) DA^{2A} is characterized by the high expression of *Slc32a1* but low expression of *Satb1*, Gsg1l, and *Clstn2*.

(D) DA^{2B} is defined by the unique coexpression of *Lpl*, *Adcyap1*, *Otx2*, and *Aldh1a1*.

(E) No distinctive marker could be identified for subtype DA^{2C}, which also possesses some similarity with DA^{1B}, if it was not for high levels of *Calb1*, *Cck*, and *Slc17a6*.

(F) DA^{2D} can be identified by the unique expression of *Vip*, combined with low expression of *Snca*, *Chrna4*, and *Ntf3*.

All error bars are SEM.

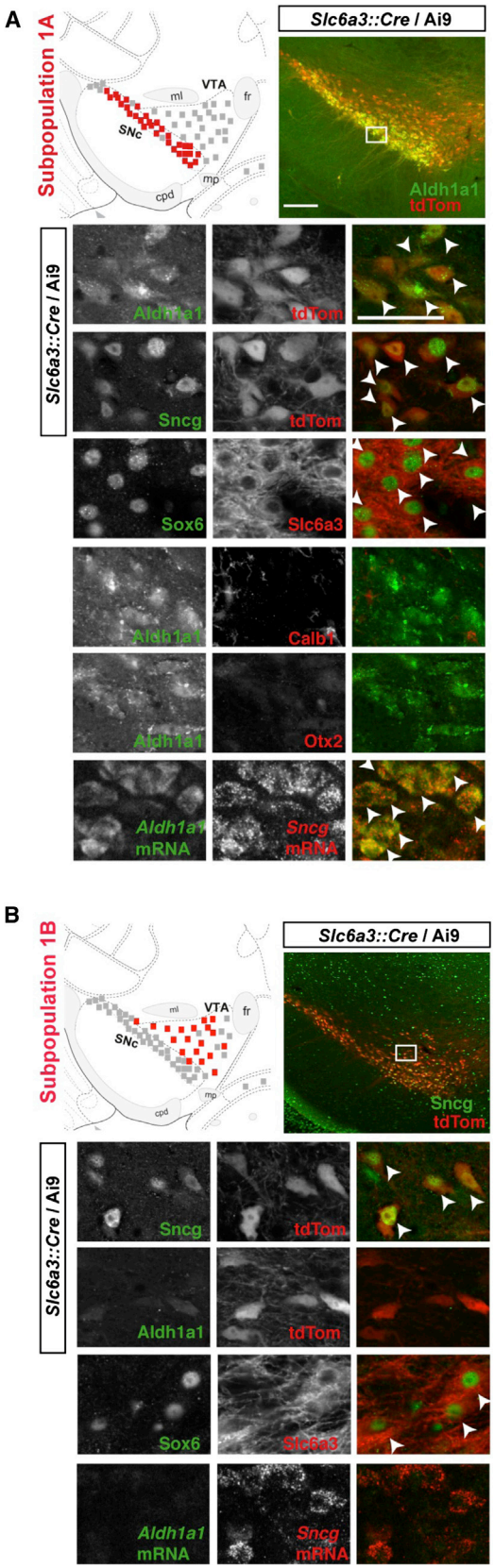

Figure 4. Molecular and Neuroanatomical Characterization of Dopamine Neuron Subtypes of the First Cluster in the Adult Brain

(A) Subtype DA^{1A} is mainly located in the SNc (red square), with a few cells observable in the RR (not shown). These neurons are positive for Aldh1a1, Sncg, and Sox6 but do not show the expression of Calb1 and Otx2.

(B) DA^{1B} subtype neurons are generally located just dorsally to DA^{1A}, encompassing the dorsal portion of the SNc and dorso-rostral VTA, as well as RR (not shown). DA^{1B} neurons can be labeled for Sncg and Sox6, but Aldh1a1 is absent in this cell population. The scale bar represents 200 μm (low magnification) and 50 μm (high magnification). Red square, five neurons mentioned population; gray square, five DA neurons.

extended amygdala in the rat (Hasue and Shammah-Lagnado, 2002; Meloni et al., 2006). Overall, the presence and absence of these markers by colabeling confirms the finding of our high-throughput single-cell qPCR study as well as validates the existence of this DA subtype with distinctive anatomical location in the PAG/DR and specific projections within the extended amygdala in the adult brain.

Finally, we found it useful to examine the expression of various classes of genes across DA subtypes (Figure S5). We found that DA subtypes exhibit distinct transcription factor profiles that could in part underlie their molecular phenotype. Additionally, neuropeptides, channels, and neurotrophic factors were substantially different between DA subtypes, suggestive of functional heterogeneity between these DA subtypes. With respect to PD-related genes, we found that these are expressed in all DA subtypes; however, *Snca* levels are increased in DA^{1A} and DA^{2B} (Figure S5D).

Relevance of Dopamine Neuron Identity to Parkinson's Disease

In Parkinson's disease, DA neurons located in the ventral tier of the SNc are particularly vulnerable (Damier et al., 1999). Thus, the DA^{1A} subtype could be of special clinical relevance, because it is located in the ventral tier of the SNc. To determine if molecular codes were linked to vulnerability, we evaluated the susceptibility of DA^{1A} neurons to the neurotoxin 1-methyl-4-phenyl-1,2,3,6-tetrahydropyridine (MPTP), commonly used to mimic a number of important pathological features of parkinsonism in mice. We observed a significant decrease in the number of midbrain Th+ cells as quantified by stereological analysis (4,039 compared to 2,352; p value < 0.01; Figure 6A). As previously reported (German et al., 1996), cells located in the SNc were particularly vulnerable (58.0% cell loss; p value < 0.0001), compared to VTA (39.9% cell loss; p value < 0.005), IF (14.3% cell loss; p value = 0.5), RR (23.4% cell loss; p value = 0.25), and CLI (43.3% cell loss; p value < 0.05). We tested the hypothesis that DA^{1A} subtype could be more vulnerable to MPTP toxin and examined the vulnerability of Aldh1a1-labeled neurons of SNc and RR (defining DA^{1A}). Indeed, *Calb1* and *Otx2* genes that have been associated to resistance to MPTP and PD are absent in this population (Di Salvio et al., 2010b; Liang et al., 1996). We found that DA^{1A} neurons were significantly more vulnerable because we observed a 66.2% diminution of Aldh1a1+ cells in the SNc and RR of MPTP-treated mice compared to animals injected with saline (Figure 6B). The remaining DA neurons were significantly less affected by MPTP, with only 39.1% DA cell loss compared to saline (p value = 0.001; Figure 6C). In comparison, DA^{2B} subtype that is defined

by the coexpression Aldh1a1 and Otx2, and is observed in the ventromedial VTA, is not differently affected by MPTP compared to other DA populations (Figure 6C). Additionally, when we counted Aldh1a1-positive and negative cells specifically in the SNc, we found that Aldh1a1+ cells (DA^{1A}) are significantly more vulnerable than Aldh1a1− (DA^{1B}) cells to MPTP (Aldha1+ showed 70% loss; Aldh1a1− showed 50% loss; p value = 0.0337). MPTP vulnerability has been in part attributed to levels of Slc6a3 (Di Salvio et al., 2010b); this latter finding is interesting as both DA^{1A} and DA^{1B} display high *Slc6a3* (Figure S5E), yet the Aldh1a1+ DA^{1A} cohort appears more vulnerable. Factors other than *Slc6a3* levels may therefore also impact DA neurons vulnerability in the MPTP model of PD.

DISCUSSION

This study demonstrates the existence of multiple molecularly distinct DA neuron subtypes using a single-cell qRT-PCR approach. These subtypes all share a core genetic program to produce the neurotransmitter dopamine, upon which subtype-specific gene-expression modules are superimposed. Our high-throughput approach identified several markers related to specific DA subpopulations and, more importantly, their coordinated expression in single cells. We show that each DA subtype has signature expression profiles of transcription factors (Figure S5B), channels (Figure S5C), receptors (Figure S5C), DA-related genes (Figure S5E), neuropeptides (Figure S5F), and secretory factors (Figure S5G). Furthermore, we show that some of these identified subtypes have distinct anatomical and functional properties. Our study applies this technology to classify, in a polythetic manner, neuron subtypes within a neurotransmitter group. Although our study focused exclusively on the DA system, a similar approach could be used to dissect other neurotransmitter systems within a defined brain region.

Heterogeneous expression of markers in the DA system has been reported (Di Salvio et al., 2010b; Dougalis et al., 2012; Fu et al., 2012; Gerfen et al., 1987; Hnasko et al., 2012; McCaffery and Dräger, 1994; Smits et al., 2013). Previous studies have relied on in situ hybridization, or antibody colabeling with Th, to localize marker expression. These studies provided an important starting point for the classification of DA neuron subtypes presented here. Because DA neurons are heterogeneous and intermingled, these approaches, whereas informative, do not provide conclusive evidence of coordinated gene expression, an essential feature of a neuronal subtype. In contrast, the approach presented here reveals coordinated expression of cohorts of genes, thus allowing the classification of DA subtypes in a polythetic manner, an important goal in the field of neuronal classification (Bota and Swanson, 2007; Fishell and Heintz, 2013).

Our study has limitations. First, our classification was achieved in early postnatal brain, at a stage when DA neurons are still immature in terms of pace-making activity (Chan et al., 2007) and glutamate receptor expression (Bellone et al., 2011). It is therefore possible that some markers on which the classification is based are specific to this developmental time point. However, the fact that we could observe all markers that we tested in the adult brain would argue that our single-cell array analysis is highly informative, despite the neonatal time point. Second, it is possible that DA neurons with low/absent Slc6a3 (Lammel et al., 2008) were excluded from these analyses, due to inefficient recombination of the reporter by *Slc6a3*::*Cre*. Third, it is possible that there are biases in the dissociation and FACS method that could disproportionately skew the numbers of each DA subtype. This could explain the discrepancy between the proportion of each subtype observed in the array, compared to what was observed in the adult by immunofluorescence and in situ hybridization, although these latter methods may also have inherent bias. Fourth, this method requires some knowledge of gene expression, in this case provided by important earlier studies (Chung et al., 2005; Greene et al., 2005; Grimm et al., 2004). Additionally, expanding the number of genes and cells sampled could increase the power of this method and could yield additional DA subtypes or further subdivide currently identified DA subtypes. Ultimately, unbiased single-cell mRNA sequencing could be used to provide further resolution for DA cell classification. Despite these limitations, this study represents an important advance; the method used here allows simultaneous, efficient, and quantitative assessment of key DA markers in single cells. Based on these coordinated gene-expression profiles, we were able to distinguish multiple molecularly distinct DA subtypes with unique properties, one with a specific projection, and one selectively vulnerable. Further work will be required to illustrate the projections, physiological characteristics, and functions of the DA subtypes defined here.

Defining DA neurons on a molecular basis will allow a better understanding of the vulnerability of selective DA neuron subsets. In PD, ventral tier SNc neurons are more vulnerable than either dorsal tier or VTA DA neurons (Damier et al., 1999). Our data suggest that the Aldh1a1 population in the ventral tier appears to be particularly vulnerable in an MPTP mouse model. It is of interest that Aldh1a1, an aldehyde dehydrogenase, is inhibited by the fungicide benomyl, for which high exposure was associated with an increased PD risk (Fitzmaurice et al., 2013). Additionally, the DA^{1A} subtype is characterized by significantly lower levels of *Foxa2* and *En1*, as well as higher levels of *Snca*, which could in part underpin selective vulnerability in dosage-sensitive backgrounds (Kittappa et al., 2007; Sgadò et al., 2006; Singleton et al., 2003). Our data therefore could offer additional insights into the selective vulnerability of DA neurons.

Understanding the molecular complexity of midbrain DA subtypes might help refine and develop new therapeutic approaches for DA-related diseases. Indeed, DA signaling and receptors are currently the main and potential target in the treatment of PD, schizophrenia, ADHD, addiction, and depression, among others. An important limitation of current DA therapies is side effects, largely due to the indiscriminate targeting of the DA system. For instance, systemic levodopa, the main treatment for PD, induces psychotic symptoms including hallucinations and impulsive behaviors in up to 40% of patients (Chou et al., 2007; Diederich et al., 2009). Conversely, typical and atypical antipsychotics display adverse effects including motor symptoms such as parkinsonism or tardive dyskinesia. Elucidating DA subtypes may help uncover novel candidates for a new generation of targeted therapeutics.

The stem cell field has highlighted the urgent need to better understand the molecular basis of DA neuron diversity toward

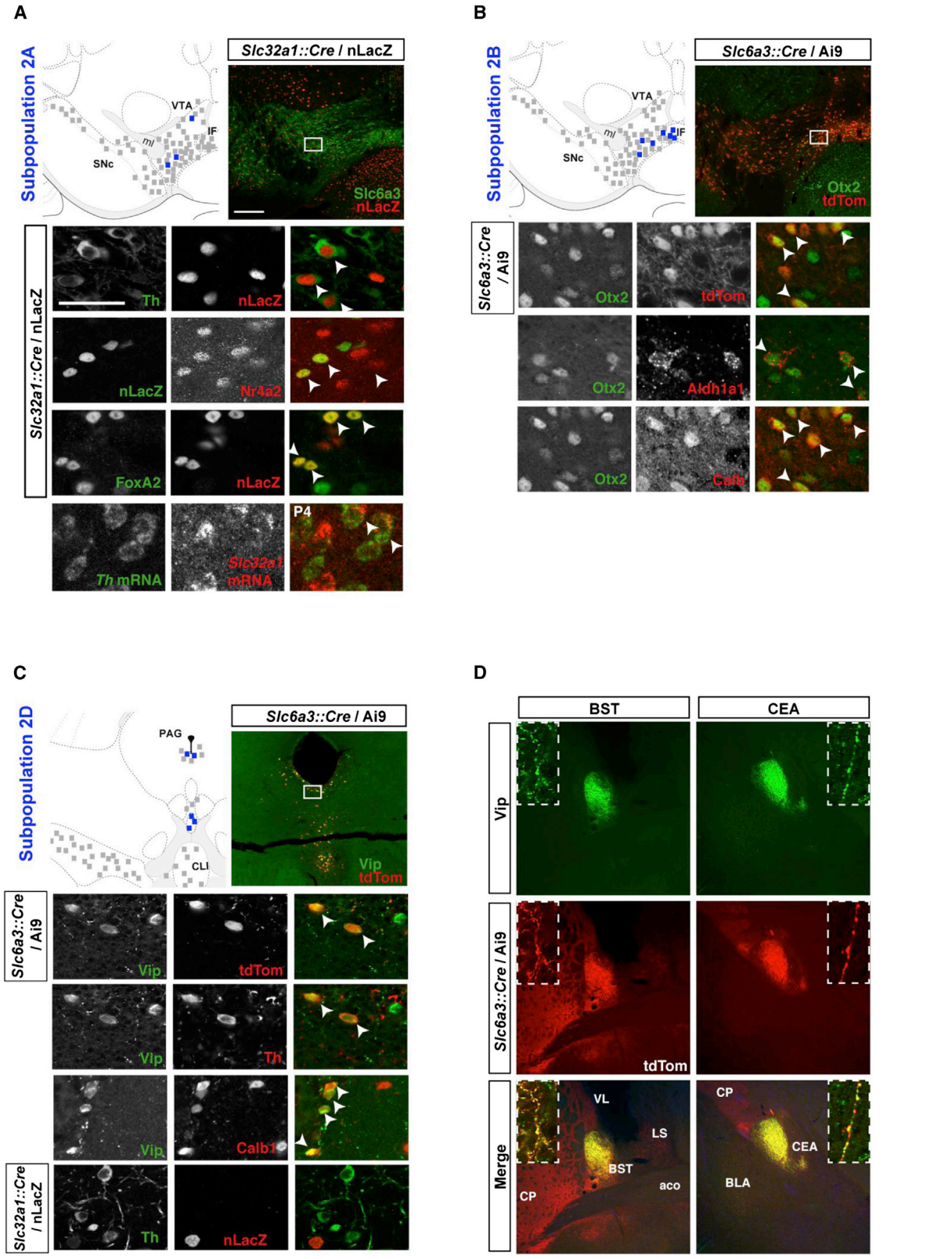

(legend on next page)

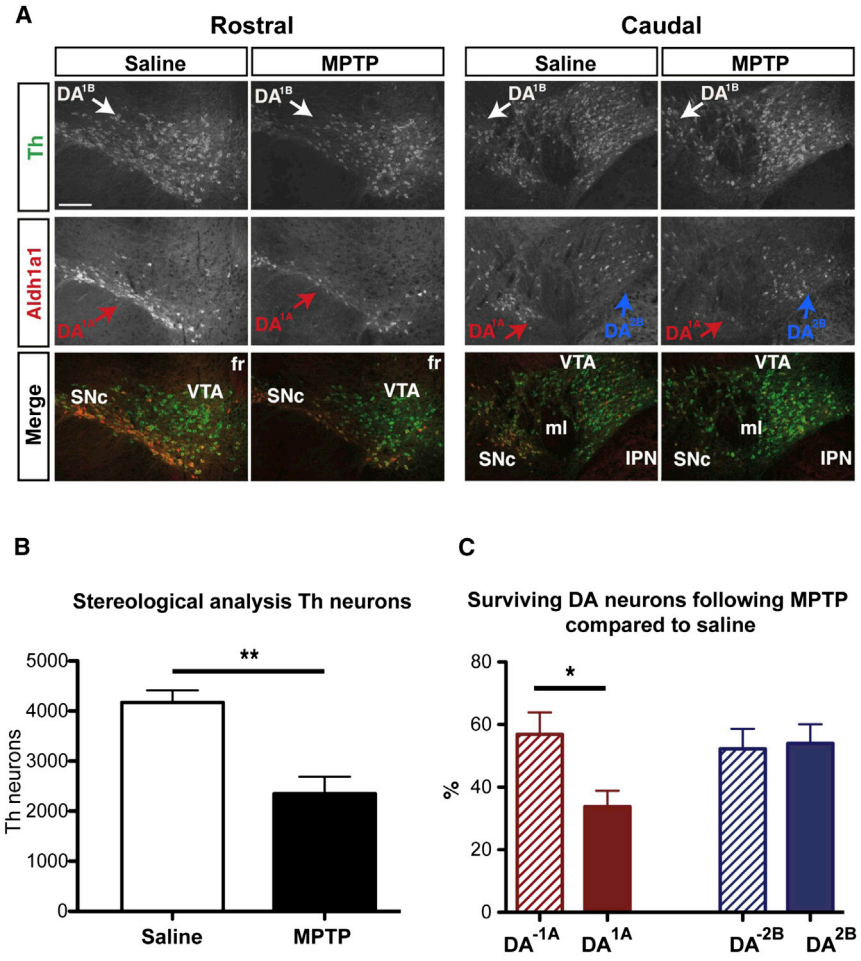

Figure 6. Dopamine Neuron DA^{1A} Subtype Is Selectively Vulnerable in an MPTP Model

(A) Example of Aldh1a1 (red) and Th (green) labeling in the midbrain of saline- and MPTP-treated animals.

(B) MPTP induced a significant reduction in Th immunoreactivity of midbrain neurons.

(C) DA^{1A} subtype is more severely affected by the toxin as compared to other DA subtypes (labeled DA^{-1A}); in contrast, DA^{2B} does not show differential vulnerability. The scale bar represents 200 μm (low magnification).

All error bars are SEM.

programming human embryonic or induced pluripotent stem cells toward specific DA fates (Studer, 2012). DA subtypes derived from stem cells would serve as more-accurate models for DA-related disease and would facilitate regenerative medicine. Our study provides a molecular barcode for several DA subtypes including subtype DA^{1A}, of great interest because of its location at the ventral aspect of the SNc and its selective vulnerability. In this regard, revisiting previous lineage analyses aimed at uncovering distinct DA lineages (Joksimovic et al., 2009) will benefit from this array of molecular markers. Additionally, our study reveals transcription factor codes that may underpin the development of DA heterogeneity (Figure S5B), which could be important for embryonic stem cell programming of DA subtypes.

Finally, the present study provides entry points that will allow genetic access to subtypes of DA neurons. However, because none of the markers used here are expressed exclusively in a DA subtype, intersectional platforms using multiple recombinase systems would be required to manipulate these subtypes in an otherwise intact brain (Awatramani et al., 2003). Provided with an appropriate Flp line, these genetic entry points could be used with mouse genetic-based platforms (Awatramani et al., 2003; Jensen et al., 2008; Kim et al., 2009; Ray et al., 2011; Robertson et al., 2013; Yamamoto et al., 2009) or more recently developed viral platforms, which allow dual recombinase mediated intersectional gene activation (Fenno et al., 2014). Projection and functional analyses following intersectional genetic labeling have been successful in dissecting the connections of serotonin and noradrenergic populations in the hindbrain (Jensen et al., 2008; Robertson et al., 2013). In the hindbrain, these neuronal populations span multiple developmentally defined rhombomeres and therefore could be dissected using developmentally defined rhombomere-specific Cre lines (Awatramani et al., 2003; Farago et al., 2006; Jensen et al., 2008; Robertson et al., 2013). In the midbrain DA system, there are no such convenient segmental divisions. Thus, our data, providing genetic entry points to defined DA subtypes, will further facilitate functional investigations using

Figure 5. Molecular and Neuroanatomical Characterization of Dopamine Neuron Subtypes of the Second Cluster in the Adult Brain

(A) Subtype DA^{2A} is uniquely defined by the expression of *Slc32a1*, here mapped using a *Slc32a1*::*Cre* mouse with a nuclear LacZ reporter (nLacZ). These cells are bona fide DA neurons, as they can be labeled for Th, Nr4a2 (Nurr1), FoxA2, and Slc6a3 (Dat). These cells are intermingled with other DA subtypes throughout the VTA.

(B) DA^{2B} neurons can be labeled with Otx2, Aldh1a1, and Calb1 but not Sox6 (not shown). These cells are positioned mainly in the ventromedial VTA and IF.

(C) Subpopulation DA^{2D} is located in the periaqueductal gray (PAG) and dorsal raphe (DR) region and can be labeled with the Vip antibody. These DA cells express Th and FoxA2 and are labeled by *Slc6a3*::*Cre* driver. These cells are also Calb1-positive but negative for Otx2, Aldh1a1, and *Slc32a1*::*Cre*.

(D) Only subset of midbrain DA neurons axonal projections, as labeled with tdTomato in *Slc6a3*::*Cre*/Ai9, colocalized with Vip. These fibers, which originate from subtype DA^{2D} form discrete projections to the oval part of the bed nucleus of the stria terminalis (BSTov) and the lateral part of the central amygdala (CEAl), with apparent boutons colocalizing Vip (green) and tdTomato (red; inset). The scale bar represents 200 μm (low magnification) and 50 μm (high magnification). Blue square, five neurons mentioned population; gray square, five DA neurons.

chemogenetic or optogenetic technology (Ray et al., 2011; Rogan and Roth, 2011; Tye and Deisseroth, 2012) as well as transcriptomic and connectomic analyses, with the ultimate goal of disentangling this pleiotropic neurotransmitter system.

EXPERIMENTAL PROCEDURES

Mice and Flow Cytometry

Mice were maintained and euthanized according to the protocols approved by the Northwestern University Animal Care and Use Committee. The *Slc6a3*::*Cre* and Ai9 mice used in this study were both maintained on C57Bl/6 background and were described previously (Bäckman et al., 2006; Madisen et al., 2010). In this mouse, the vast majority of DA neurons are recombined. For the single-cell study, the midbrain of three P4 mice were carefully dissected to grossly the size of 1 × 2 × 2 mm. Midbrain neurons were dissociated using Papain Dissociation System (Worthington Biochemical Corporation) according to the manufacturer's instructions. Cells were resuspended in Neurobasal medium (Life Technologies), and single cells were immediately sorted in a 96-well plate with the help of Northwestern University Flow Cytometry Facility and a Cancer Center Support Grant (NCI CA060553). FACS was performed on an Aria II SORP sorter using a fine-tune sort precision protocol. This approach provides a reliable single-cell sorting by adequately calculating the drop delay but also increases the proportion of empty wells. Three 96-well plates for gene-expression analysis were filled with single fluorescently labeled neurons, with the exception of six wells that were used for calibration curves, three wells used for positive control (10, 20, and 50 cells) and one well used for negative control (e.g., Figure S1). For immunofluorescence and fluorescence in situ hybridization, perfused adult mice (older than P56) were used unless stated otherwise.

Primers Design and Validation

Each primer pair was designed, generated, and experimentally validated by Fluidigm. Primers were designed to span exon junctions, when possible, with an average amplicon size of 82 bp (Table S1). Assay performance was evaluated via serial dilution of a commercial reference sample. The ΔCT (or Cq) was calculated for all pairwise combinations of assays and the slope of ΔCT versus log2 template dilution calculated and averaged. The mean slope of ΔCT versus template concentration for cDNA templates indicates relative error in measuring 2-fold changes for the given assay compared to the other assays (Schmittgen and Livak, 2008). If two assays have equal efficiencies and there is no measurement error, the slope will be zero. Overall, 98.9% of assays fell in the range of −0.1 and 0.1.

Single-Cell Gene-Expression qPCR

Cells were sorted directly into 5 μl of the reverse transcription (RT) mix solution 1, composed of 1.2 μl VILO Reaction Mix (SuperScript VILO cDNA Synthesis Kit; Life Technologies), 0.3 μl 20 U/μl SUPERase-In, 0.25 μl NP-40 Detergent Surfact-Amps Solution (Fisher Scientific), and 3.25 μl of nuclease-free H_2O (Teknova). RNA was denatured 90 s at 65°C. The plate was quickly chilled on ice for 5 min and centrifuged briefly at 4°C. We added 1 μl to each well of RT mix solution 2 composed of 0.15 μl of 10× SuperScript Enzyme Mix, 0.12 μl of T4 Gene 32 Protein (New England Biolabs), and 0.73 μl of nuclease-free H_2O. Reverse transcription was carried out in thermal cycler under the following condition: 5 min at 25°C, 30 min at 50°C, 25 min at 55°C, 5 min at 60°C, and 10 min at 70°C. Subsequently, in the same tube, cDNA went through sequence-specific amplification by denaturing at 95°C for 15 s and annealing and amplification at 60°C for 4 min for 18 cycles. These preamplified products were diluted 5-fold prior to the analysis with Universal PCR Master Mix and inventoried TaqMan gene-expression assays (ABI) in 96.96 Dynamic Arrays on a BioMark System (Fluidigm). Ct values were calculated from the system's software (BioMark Real-time PCR Analysis; Fluidigm). For quality control, the melt curve was established and all peaks falling outside user-defined threshold were removed from analysis (Figure S2).

Single-Cell Data Processing and Analysis

Overall, 274 single-cell were sorted into 96-well plates. Out of these cells, we removed cells with weak or no expression of *Gapdh*, defined by greater than two SDs from the median, from the analysis. In addition, we removed cells with weak expression of genes defining DA neurons (Ddc, *Th*, *Slc6a3*, and *Slc18a2*) using the same criteria. These cells were assumed to be non-DA cells and were removed from the analysis, leaving a final 159 DA neurons to be further analyzed. In addition, despite depicting a normal standard curve, two genes, *Pvalb* and *Aldh1a2*, were undetectable in all cells analyzed, and these genes were thus excluded from further analysis and replaced by the housekeeping genes *Actb* and *Hprt*. All Ct values (e.g., Figure S1) obtained from the BioMark System were converted into relative expression levels by subtracting the values from the threshold value of 24 (Figures 1B and S3). All Ct values above 24 were considered below detectability level. As the Ct scale is logarithmic (a difference of one Ct corresponds to a doubling of measured transcript), the values obtained were normalized to the endogenous control by subtracting, for each cell, its *Gapdh* Ct value (delta Ct). The fold difference was obtained by using the highest gene expression cell sample for each gene and used as a reference to calculate the delta delta Ct (comparative Ct method). In order to group cells with similar expression profile, we used cluster analysis by correlation coefficient similarity on logarithmic expression data. Cells were assigned to a specific DA subtype based on this cluster analysis. To compare gene expression level between identified populations, because the homogeneity of variance assumption was violated, normalized gene levels between subtypes were compared between DA subtypes using a Kruskal-Wallis and Dunn's post hoc analysis with Bonferroni correction of alpha value.

Immunofluorescence

Staining was performed on adult (more than 2 months of age) wild-type and *Slc6a3*::*Cre*; Ai9 mice for minimum of n = 3 for all antibodies. To map the DA^{2A} subtype, we crossed a mouse in which Cre was knocked in *Slc32a1* locus (Vong et al., 2011), with a Rosa locus reporter in which a floxed stop cassette was followed by nuclear LacZ RosaNZG (Yamamoto et al., 2009). Mice were perfused with cold 4% paraformaldehyde (PFA) in PBS, and the brains were dissected and fixed overnight in the same solution, cryoprotected in 30% sucrose PBS solution, and sectioned at 25 μm using a freezing microtome. Tissue sections were stained with the following primary antibodies: mouse anti-Calbindin (Sigma-Aldrich; 1:1,000), rabbit anti-Calbindin (Chemicon; 1:500), rat anti-Dat (Santa Cruz Biotechnology; 1:50), goat anti-FoxA2 (Santa Cruz; 1:50), goat anti-LacZ (Biogenesis; 1:1,500), rabbit anti-LacZ (Cappel; 1:1,500), rabbit anti-Nr4a2 (Santa Cruz; 1:500), goat anti-Otx2 (Neuromics; 1:200), rabbit anti-Aldh1a1 (Abcam; 1:200), rabbit anti-Sncg (Abcam; 1:1,000), rabbit anti-Sox6 (Abcam; 1:500), rabbit anti-Vip (Abcam; 1:500), rabbit anti-SatB1 (Abcam; 1:1,000), and sheep anti-TH (Pel-Freez; 1:300). Sections were imaged by confocal microscopy (Leica DM6000 CFS). For each DA subtype mapped in Figures 4 and 5, a combination of markers specific to this subtype was analyzed. Cells were counted on representative sections, superimposed to the reference section from the Allen Brain Atlas, and averaged across animals. Each colored square in Figures 4 and 5 represents five neurons of the DA subtype at the approximate location, whereas each gray square represents five DA neurons of another subtype.

Fluorescent In Situ Hybridization

Fluorescent in situ hybridization (ISH) was performed with single-stranded digoxigenin (Roche) and fluorescein-labeled riboprobes directed against the following mRNAs: *Th* (GenBank accession number: NM_009377), *Aldh1a1* (NM_013467), *Ndnf* (A930038C07Rik), *Slc32a1* (GenBank accession number: NM_009508), and *Sncg* (GenBank accession number: NM_011430). The ISH protocol was adapted from Joksimovic et al. (2009).

MPTP Protocol

Adult C57BL/6 mice (n = 16) received four intraperitoneal (i.p.) injections of freshly diluted MPTP-HCl (20 mg/kg; Sigma) dissolved in saline 0.9%. MPTP was administered in an acute manner at 2 hr intervals as previously described (Jackson-Lewis and Przedborski, 2007). Remaining animals (n = 8) received i.p. vehicle injections at the time of MPTP administration. Mice were sacrificed 7 days following the last MPTP injection through intracardiac perfusion with either PBS 0.1 M only or PBS followed by PFA 4%. Brains were collected, further fixed in PFA, and cryoprotected in 20% sucrose.

SUPPLEMENTAL INFORMATION

Supplemental Information includes six figures and one table and can be found with this article online at http://dx.doi.org/10.1016/j.celrep.2014.10.008.

AUTHOR CONTRIBUTIONS

J.-F.P. designed and performed the experiments and wrote the manuscript, J.Z. performed several colabeling experiments, J.D.-O. and F.C. provided MPTP-treated brain sections and initial analysis, K.-Y.A.K. helped with statistical analysis, and R.B.A. supervised the study and helped write the manuscript.

ACKNOWLEDGMENTS

The authors would like to thank Jennifer Darnell and Jason McKinney (Fluidigm) for technical assistance. The authors thank Dr. Richard J. Miller and Dr. D. James Surmeier for useful comments on the manuscript. This research was supported by R21 (1R21NS072703-01) and Northwestern Memorial Foundation (Paul Ruby Foundation for Parkinson's Research) grants to R.B.A. This research was also supported by FRSQ, MJFF, and CIHR grants to J.-F.P.; a Paul Ruby Foundation grant to J.Z.; and a FRSQ grant to J.D.-O. K.-Y.A.K. would like to acknowledge NIH CTSA funding to Northwestern University Feinberg School of Medicine (UL1 TR000150 and UL1 RR025741). F.C. is a recipient of a National Research Career award from the Fonds de Recherche du Québec en Santé, providing salary support and funding.

Received: June 16, 2014
Revised: August 7, 2014
Accepted: September 30, 2014
Published: October 30, 2014

REFERENCES

Ang, S.-L. (2006). Transcriptional control of midbrain dopaminergic neuron development. Development *133*, 3499–3506.

Arlotta, P., Molyneaux, B.J., Chen, J., Inoue, J., Kominami, R., and Macklis, J.D. (2005). Neuronal subtype-specific genes that control corticospinal motor neuron development in vivo. Neuron *45*, 207–221.

Awatramani, R., Soriano, P., Rodriguez, C., Mai, J.J., and Dymecki, S.M. (2003). Cryptic boundaries in roof plate and choroid plexus identified by intersectional gene activation. Nat. Genet. *35*, 70–75.

Bäckman, C.M., Malik, N., Zhang, Y., Shan, L., Grinberg, A., Hoffer, B.J., Westphal, H., and Tomac, A.C. (2006). Characterization of a mouse strain expressing Cre recombinase from the 3′ untranslated region of the dopamine transporter locus. Genesis *44*, 383–390.

Bellone, C., Mameli, M., and Lüscher, C. (2011). In utero exposure to cocaine delays postnatal synaptic maturation of glutamatergic transmission in the VTA. Nat. Neurosci. *14*, 1439–1446.

Blaess, S., Bodea, G.O., Kabanova, A., Chanet, S., Mugniery, E., Derouiche, A., Stephen, D., and Joyner, A.L. (2011). Temporal-spatial changes in Sonic Hedgehog expression and signaling reveal different potentials of ventral mesencephalic progenitors to populate distinct ventral midbrain nuclei. Neural Dev. *6*, 29.

Bota, M., and Swanson, L.W. (2007). The neuron classification problem. Brain Res. Brain Res. Rev. *56*, 79–88.

Buganim, Y., Faddah, D.A., Cheng, A.W., Itskovich, E., Markoulaki, S., Ganz, K., Klemm, S.L., van Oudenaarden, A., and Jaenisch, R. (2012). Single-cell expression analyses during cellular reprogramming reveal an early stochastic and a late hierarchic phase. Cell *150*, 1209–1222.

Chan, C.S., Guzman, J.N., Ilijic, E., Mercer, J.N., Rick, C., Tkatch, T., Meredith, G.E., and Surmeier, D.J. (2007). 'Rejuvenation' protects neurons in mouse models of Parkinson's disease. Nature *447*, 1081–1086.

Chou, K.L., Borek, L.L., and Friedman, J.H. (2007). The management of psychosis in movement disorder patients. Expert Opin. Pharmacother. *8*, 935–943.

Chung, C.Y., Seo, H., Sonntag, K.C., Brooks, A., Lin, L., and Isacson, O. (2005). Cell type-specific gene expression of midbrain dopaminergic neurons reveals molecules involved in their vulnerability and protection. Hum. Mol. Genet. *14*, 1709–1725.

Chung, C.Y., Licznerski, P., Alavian, K.N., Simeone, A., Lin, Z., Martin, E., Vance, J., and Isacson, O. (2010). The transcription factor orthodenticle homeobox 2 influences axonal projections and vulnerability of midbrain dopaminergic neurons. Brain *133*, 2022–2031.

Damier, P., Hirsch, E.C., Agid, Y., and Graybiel, A.M. (1999). The substantia nigra of the human brain. II. Patterns of loss of dopamine-containing neurons in Parkinson's disease. Brain *122*, 1437–1448.

Darvas, M., and Palmiter, R.D. (2009). Restriction of dopamine signaling to the dorsolateral striatum is sufficient for many cognitive behaviors. Proc. Natl. Acad. Sci. USA *106*, 14664–14669.

Di Salvio, M., Di Giovannantonio, L.G., Omodei, D., Acampora, D., and Simeone, A. (2010a). Otx2 expression is restricted to dopaminergic neurons of the ventral tegmental area in the adult brain. Int. J. Dev. Biol. *54*, 939–945.

Di Salvio, M., Di Giovannantonio, L.G., Acampora, D., Prosperi, R., Omodei, D., Prakash, N., Wurst, W., and Simeone, A. (2010b). Otx2 controls neuron subtype identity in ventral tegmental area and antagonizes vulnerability to MPTP. Nat. Neurosci. *13*, 1481–1488.

Diederich, N.J., Fénelon, G., Stebbins, G., and Goetz, C.G. (2009). Hallucinations in Parkinson disease. Nat Rev Neurol *5*, 331–342.

Dougalis, A.G., Matthews, G.A.C., Bishop, M.W., Brischoux, F., Kobayashi, K., and Ungless, M.A. (2012). Functional properties of dopamine neurons and co-expression of vasoactive intestinal polypeptide in the dorsal raphe nucleus and ventro-lateral periaqueductal grey. Eur. J. Neurosci. *36*, 3322–3332.

Ekstrand, M.I., Nectow, A.R., Knight, Z.A., Latcha, K.N., Pomeranz, L.E., and Friedman, J.M. (2014). Molecular profiling of neurons based on connectivity. Cell *157*, 1230–1242.

Farago, A.F., Awatramani, R.B., and Dymecki, S.M. (2006). Assembly of the brainstem cochlear nuclear complex is revealed by intersectional and subtractive genetic fate maps. Neuron *50*, 205–218.

Fenno, L.E., Mattis, J., Ramakrishnan, C., Hyun, M., Lee, S.Y., He, M., Tucciarone, J., Selimbeyoglu, A., Berndt, A., Grosenick, L., et al. (2014). Targeting cells with single vectors using multiple-feature Boolean logic. Nat. Methods *11*, 763–772.

Fishell, G., and Heintz, N. (2013). The neuron identity problem: form meets function. Neuron *80*, 602–612.

Fitzmaurice, A.G., Rhodes, S.L., Lulla, A., Murphy, N.P., Lam, H.A., O'Donnell, K.C., Barnhill, L., Casida, J.E., Cockburn, M., Sagasti, A., et al. (2013). Aldehyde dehydrogenase inhibition as a pathogenic mechanism in Parkinson disease. Proc. Natl. Acad. Sci. USA *110*, 636–641.

Fu, Y., Yuan, Y., Halliday, G., Rusznák, Z., Watson, C., and Paxinos, G. (2012). A cytoarchitectonic and chemoarchitectonic analysis of the dopamine cell groups in the substantia nigra, ventral tegmental area, and retrorubral field in the mouse. Brain Struct. Funct. *217*, 591–612.

Gerfen, C.R., Baimbridge, K.G., and Thibault, J. (1987). The neostriatal mosaic: III. Biochemical and developmental dissociation of patch-matrix mesostriatal systems. J. Neurosci. *7*, 3935–3944.

German, D.C., Nelson, E.L., Liang, C.L., Speciale, S.G., Sinton, C.M., and Sonsalla, P.K. (1996). The neurotoxin MPTP causes degeneration of specific nucleus A8, A9 and A10 dopaminergic neurons in the mouse. Neurodegeneration *5*, 299–312.

Greene, J.G., Dingledine, R., and Greenamyre, J.T. (2005). Gene expression profiling of rat midbrain dopamine neurons: implications for selective vulnerability in parkinsonism. Neurobiol. Dis. *18*, 19–31.

Grimm, J., Mueller, A., Hefti, F., and Rosenthal, A. (2004). Molecular basis for catecholaminergic neuron diversity. Proc. Natl. Acad. Sci. USA *101*, 13891–13896.

Guo, G., Huss, M., Tong, G.Q., Wang, C., Li Sun, L., Clarke, N.D., and Robson, P. (2010). Resolution of cell fate decisions revealed by single-cell gene expression analysis from zygote to blastocyst. Dev. Cell *18*, 675–685.

Guzman, J.N., Sanchez-Padilla, J., Wokosin, D., Kondapalli, J., Ilijic, E., Schumacker, P.T., and Surmeier, D.J. (2010). Oxidant stress evoked by pacemaking in dopaminergic neurons is attenuated by DJ-1. Nature *468*, 696–700.

Hasue, R.H., and Shammah-Lagnado, S.J. (2002). Origin of the dopaminergic innervation of the central extended amygdala and accumbens shell: a combined retrograde tracing and immunohistochemical study in the rat. J. Comp. Neurol. *454*, 15–33.

Hayes, L., Zhang, Z., Albert, P., Zervas, M., and Ahn, S. (2011). Timing of Sonic hedgehog and Gli1 expression segregates midbrain dopamine neurons. J. Comp. Neurol. *519*, 3001–3018.

Hnasko, T.S., Hjelmstad, G.O., Fields, H.L., and Edwards, R.H. (2012). Ventral tegmental area glutamate neurons: electrophysiological properties and projections. J. Neurosci. *32*, 15076–15085.

Hoekstra, E.J., von Oerthel, L., van der Linden, A.J., Schellevis, R.D., Scheppink, G., Holstege, F.C., Groot-Koerkamp, M.J., van der Heide, L.P., and Smidt, M.P. (2013). Lmx1a is an activator of Rgs4 and Grb10 and is responsible for the correct specification of rostral and medial mdDA neurons. Eur. J. Neurosci. *37*, 23–32.

Jackson-Lewis, V., and Przedborski, S. (2007). Protocol for the MPTP mouse model of Parkinson's disease. Nat. Protoc. *2*, 141–151.

Jensen, P., Farago, A.F., Awatramani, R.B., Scott, M.M., Deneris, E.S., and Dymecki, S.M. (2008). Redefining the serotonergic system by genetic lineage. Nat. Neurosci. *11*, 417–419.

Joksimovic, M., Anderegg, A., Roy, A., Campochiaro, L., Yun, B., Kittappa, R., McKay, R., and Awatramani, R. (2009). Spatiotemporally separable Shh domains in the midbrain define distinct dopaminergic progenitor pools. Proc. Natl. Acad. Sci. USA *106*, 19185–19190.

Kepecs, A., and Fishell, G. (2014). Interneuron cell types are fit to function. Nature *505*, 318–326.

Kim, J.C., Cook, M.N., Carey, M.R., Shen, C., Regehr, W.G., and Dymecki, S.M. (2009). Linking genetically defined neurons to behavior through a broadly applicable silencing allele. Neuron *63*, 305–315.

Kittappa, R., Chang, W.W., Awatramani, R.B., and McKay, R.D.G. (2007). The foxa2 gene controls the birth and spontaneous degeneration of dopamine neurons in old age. PLoS Biol. *5*, e325.

Lammel, S., Hetzel, A., Häckel, O., Jones, I., Liss, B., and Roeper, J. (2008). Unique properties of mesoprefrontal neurons within a dual mesocorticolimbic dopamine system. Neuron *57*, 760–773.

Lammel, S., Lim, B.K., Ran, C., Huang, K.W., Betley, M.J., Tye, K.M., Deisseroth, K., and Malenka, R.C. (2012). Input-specific control of reward and aversion in the ventral tegmental area. Nature *491*, 212–217.

Liang, C.L., Sinton, C.M., Sonsalla, P.K., and German, D.C. (1996). Midbrain dopaminergic neurons in the mouse that contain calbindin-D28k exhibit reduced vulnerability to MPTP-induced neurodegeneration. Neurodegeneration *5*, 313–318.

Macaulay, I.C., and Voet, T. (2014). Single cell genomics: advances and future perspectives. PLoS Genet. *10*, e1004126.

Madisen, L., Zwingman, T.A., Sunkin, S.M., Oh, S.W., Zariwala, H.A., Gu, H., Ng, L.L., Palmiter, R.D., Hawrylycz, M.J., Jones, A.R., et al. (2010). A robust and high-throughput Cre reporting and characterization system for the whole mouse brain. Nat. Neurosci. *13*, 133–140.

Margolis, E.B., Lock, H., Chefer, V.I., Shippenberg, T.S., Hjelmstad, G.O., and Fields, H.L. (2006a). Kappa opioids selectively control dopaminergic neurons projecting to the prefrontal cortex. Proc. Natl. Acad. Sci. USA *103*, 2938–2942.

Margolis, E.B., Lock, H., Hjelmstad, G.O., and Fields, H.L. (2006b). The ventral tegmental area revisited: is there an electrophysiological marker for dopaminergic neurons? J. Physiol. *577*, 907–924.

McCaffery, P., and Dräger, U.C. (1994). High levels of a retinoic acid-generating dehydrogenase in the meso-telencephalic dopamine system. Proc. Natl. Acad. Sci. USA *91*, 7772–7776.

Meloni, E.G., Gerety, L.P., Knoll, A.T., Cohen, B.M., and Carlezon, W.A., Jr. (2006). Behavioral and anatomical interactions between dopamine and corticotropin-releasing factor in the rat. J. Neurosci. *26*, 3855–3863.

Ng, L., Bernard, A., Lau, C., Overly, C.C., Dong, H.-W., Kuan, C., Pathak, S., Sunkin, S.M., Dang, C., Bohland, J.W., et al. (2009). An anatomic gene expression atlas of the adult mouse brain. Nat. Neurosci. *12*, 356–362.

Ray, R.S., Corcoran, A.E., Brust, R.D., Kim, J.C., Richerson, G.B., Nattie, E., and Dymecki, S.M. (2011). Impaired respiratory and body temperature control upon acute serotonergic neuron inhibition. Science *333*, 637–642.

Robertson, S.D., Plummer, N.W., de Marchena, J., and Jensen, P. (2013). Developmental origins of central norepinephrine neuron diversity. Nat. Neurosci. *16*, 1016–1023.

Rogan, S.C., and Roth, B.L. (2011). Remote control of neuronal signaling. Pharmacol. Rev. *63*, 291–315.

Schmittgen, T.D., and Livak, K.J. (2008). Analyzing real-time PCR data by the comparative C(T) method. Nat. Protoc. *3*, 1101–1108.

Sgadò, P., Albéri, L., Gherbassi, D., Galasso, S.L., Ramakers, G.M., Alavian, K.N., Smidt, M.P., Dyck, R.H., and Simon, H.H. (2006). Slow progressive degeneration of nigral dopaminergic neurons in postnatal Engrailed mutant mice. Proc. Natl. Acad. Sci. USA *103*, 15242–15247.

Shimogori, T., Lee, D.A., Miranda-Angulo, A., Yang, Y., Wang, H., Jiang, L., Yoshida, A.C., Kataoka, A., Mashiko, H., Avetisyan, M., et al. (2010). A genomic atlas of mouse hypothalamic development. Nat. Neurosci. *13*, 767–775.

Siegert, S., Scherf, B.G., Del Punta, K., Didkovsky, N., Heintz, N., and Roska, B. (2009). Genetic address book for retinal cell types. Nat. Neurosci. *12*, 1197–1204.

Singleton, A.B., Farrer, M., Johnson, J., Singleton, A., Hague, S., Kachergus, J., Hulihan, M., Peuralinna, T., Dutra, A., Nussbaum, R., et al. (2003). alpha-Synuclein locus triplication causes Parkinson's disease. Science *302*, 841.

Smidt, M.P., and Burbach, J.P.H. (2007). How to make a mesodiencephalic dopaminergic neuron. Nat. Rev. Neurosci. *8*, 21–32.

Smits, S.M., von Oerthel, L., Hoekstra, E.J., Burbach, J.P., and Smidt, M.P. (2013). Molecular marker differences relate to developmental position and subsets of mesodiencephalic dopaminergic neurons. PLoS ONE *8*, e76037.

Stamatakis, A.M., Jennings, J.H., Ung, R.L., Blair, G.A., Weinberg, R.J., Neve, R.L., Boyce, F., Mattis, J., Ramakrishnan, C., Deisseroth, K., and Stuber, G.D. (2013). A unique population of ventral tegmental area neurons inhibits the lateral habenula to promote reward. Neuron *80*, 1039–1053.

Studer, L. (2012). Derivation of dopaminergic neurons from pluripotent stem cells. Prog. Brain Res. *200*, 243–263.

Tang, F., Barbacioru, C., Nordman, E., Li, B., Xu, N., Bashkirov, V.I., Lao, K., and Surani, M.A. (2010). RNA-Seq analysis to capture the transcriptome landscape of a single cell. Nat. Protoc. *5*, 516–535.

Tye, K.M.K., and Deisseroth, K. (2012). Optogenetic investigation of neural circuits underlying brain disease in animal models. Nat. Rev. Neurosci. *13*, 251–266.

Tye, K.M., Prakash, R., Kim, S.-Y., Fenno, L.E., Grosenick, L., Zarabi, H., Thompson, K.R., Gradinaru, V., Ramakrishnan, C., and Deisseroth, K. (2011). Amygdala circuitry mediating reversible and bidirectional control of anxiety. Nature *471*, 358–362.

Veenvliet, J.V., Dos Santos, M.T., Kouwenhoven, W.M., von Oerthel, L., Lim, J.L., van der Linden, A.J., Koerkamp, M.J., Holstege, F.C., and Smidt, M.P. (2013). Specification of dopaminergic subsets involves interplay of En1 and Pitx3. Development *140*, 3373–3384.

Vong, L., Ye, C., Yang, Z., Choi, B., Chua, S., Jr., and Lowell, B.B. (2011). Leptin action on GABAergic neurons prevents obesity and reduces inhibitory tone to POMC neurons. Neuron *71*, 142–154.

Wallén, A., Zetterström, R.H., Solomin, L., Arvidsson, M., Olson, L., and Perlmann, T. (1999). Fate of mesencephalic AHD2-expressing dopamine progenitor cells in NURR1 mutant mice. Exp. Cell Res. *253*, 737–746.

Xue, Z., Huang, K., Cai, C., Cai, L., Jiang, C.-Y., Feng, Y., Liu, Z., Zeng, Q., Cheng, L., Sun, Y.E., et al. (2013). Genetic programs in human and mouse early embryos revealed by single-cell RNA sequencing. Nature *500*, 593–597.

Yamamoto, M., Shook, N.A., Kanisicak, O., Yamamoto, S., Wosczyna, M.N., Camp, J.R., and Goldhamer, D.J. (2009). A multifunctional reporter mouse line for Cre- and FLP-dependent lineage analysis. Genesis *47*, 107–114.

Note Added in Proof

While this paper was in revision, three other manuscripts relevant to this general topic were published. These include the following:

Liu, G., Yu, J., Ding, J., Xie, C., Sun, L., Rudenko, I., Zheng, W., Sastry, N., Luo, J., Rudow, G., et al. (2014). Aldehyde dehydrogenase 1 defines and protects a nigrostriatal dopaminergic neuron subpopulation. J. Clin. Invest. *124*, 3032–3046.

Panman, L., Papathanou, M., Laguna, A., Oosterveen, T., Volakakis, N., Acampora, D., Kurtsdotter, I., Yoshitake, T., Kehr, J., Joodmardi, E., et al. (2014). Sox6 and Otx2 control the specification of substantia nigra and ventral tegmental area dopamine neurons. Cell Rep. *8*, 1018–1025.

Root, D.H., Mejias-Aponte, C.A., Zhang, S., Wang, H.-L., Hoffman, A.F., Lupica, C.R., and Morales, M. (2014). Single rodent mesohabenular axons release glutamate and GABA. Nat. Neurosci. Published online September 21, 2014. http://dx.doi.org/10.1038/nn.3823.